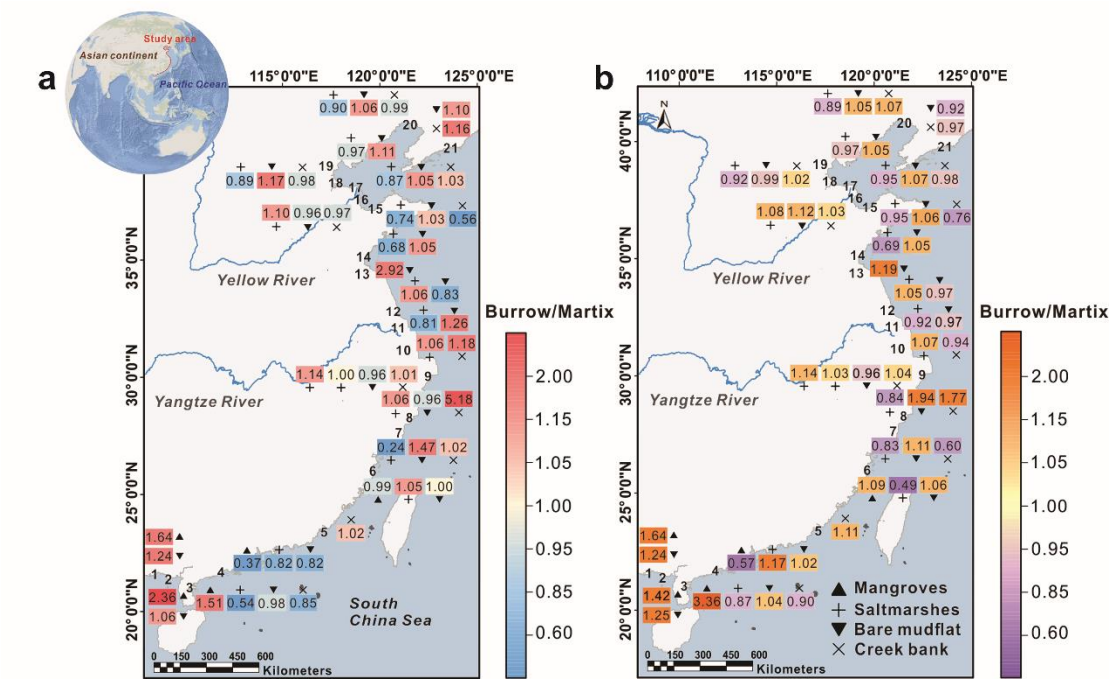

Supplementary Figure 1 | Ratio of Fe and Mn minerals between crab burrows and sediment matrix along the Chinese coast. Color gradients indicate the ratio of mineral contents between crab burrows and the sediment matrix.

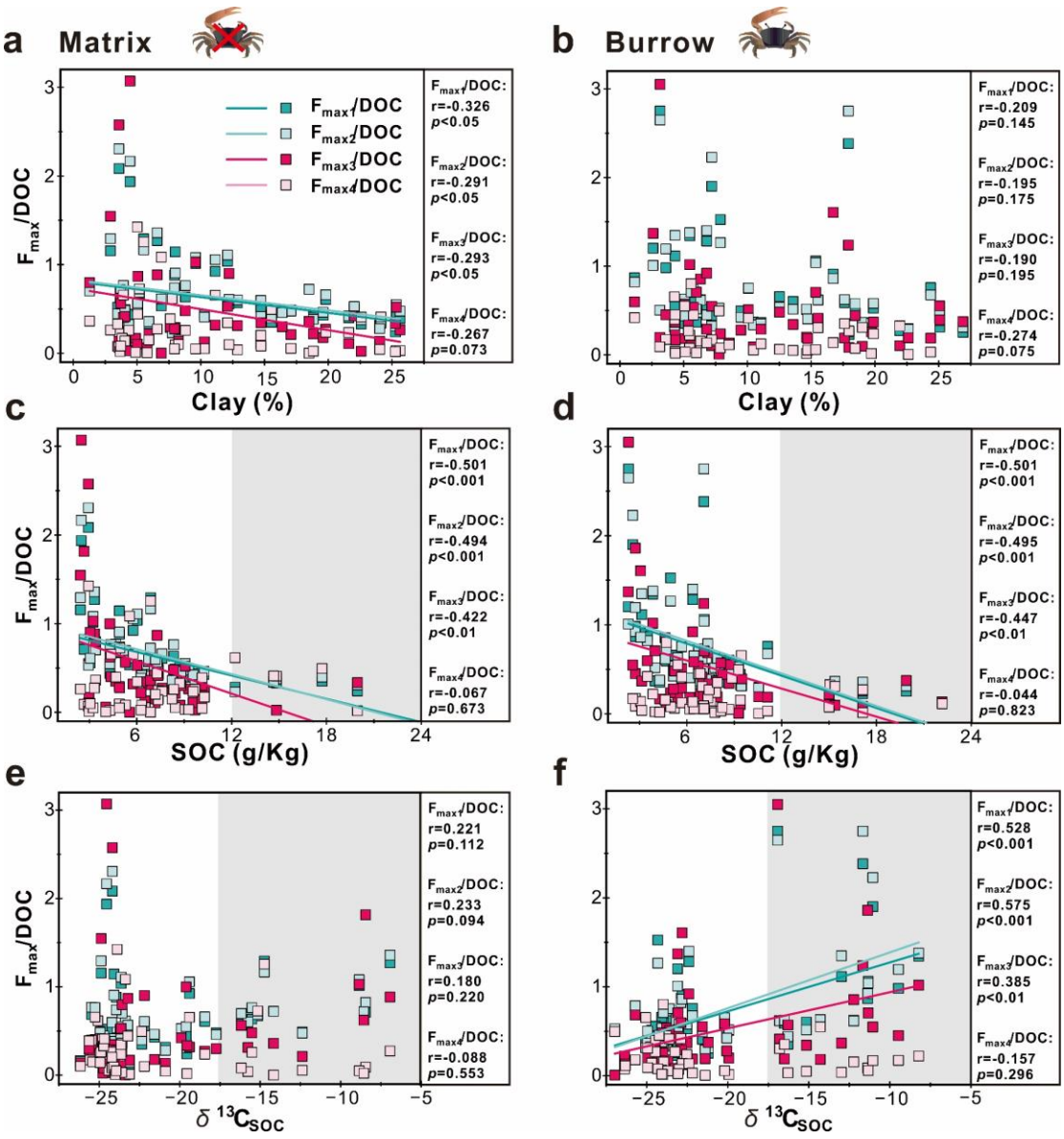

Supplementary Figure 2 | Correlations of F_{max}/DOC with clay content (%), SOC, and $\delta^{13}C_{SOC}$ in the (a, c, e) sediment matrix and (b, d, f) crab burrows. The F_{max}/DOC ratio indicates the abundance of various types of fluorescent component in the DOM[1].

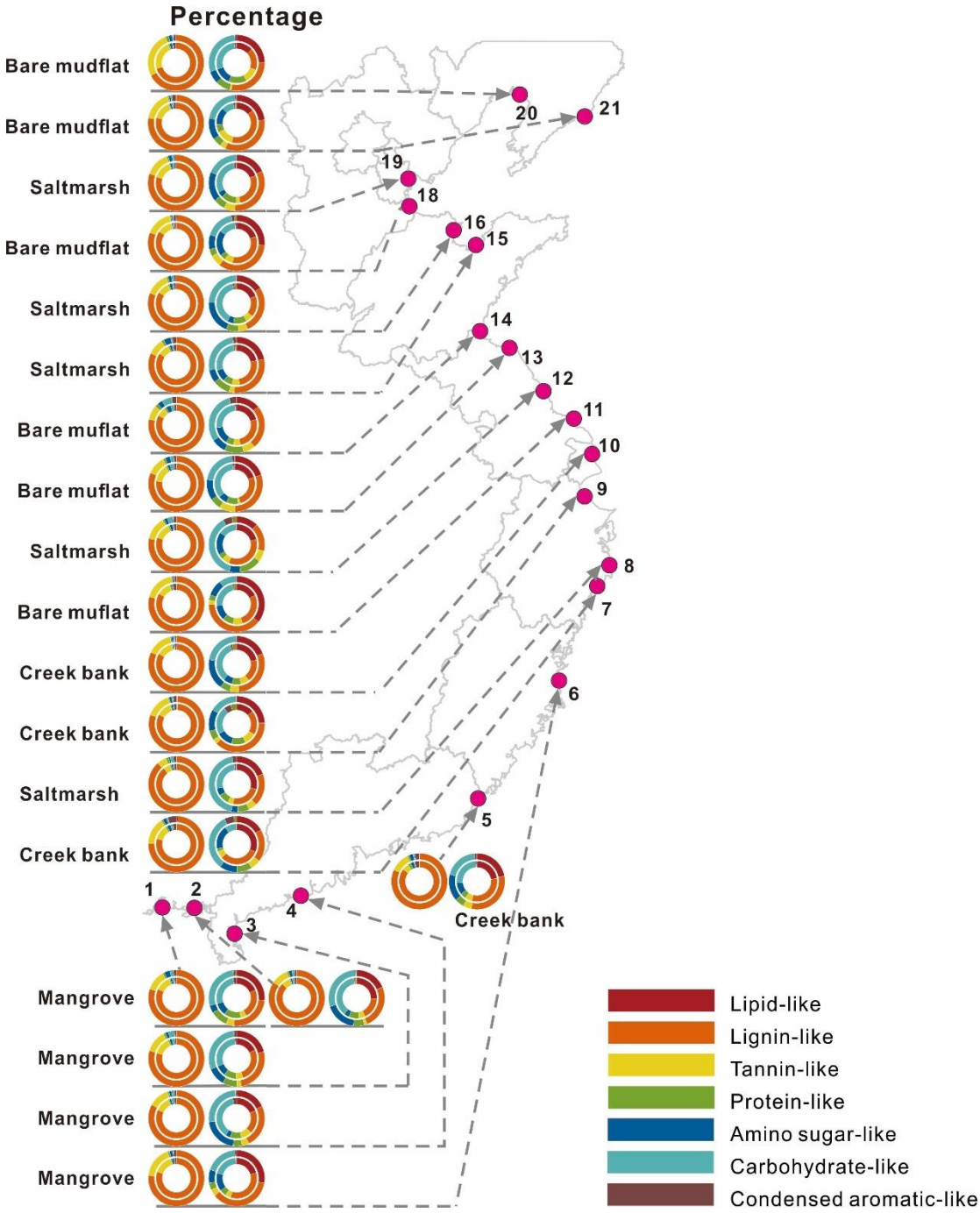

Supplementary Figure 3 | Percentage of mass peak intensities in the biochemical groups. The circles in the first column represent molecules in both the matrix and burrows, and the circles in the second column represent molecules unique to either the matrix or burrows. The outer and inner circles indicate the matrix and burrow, respectively.

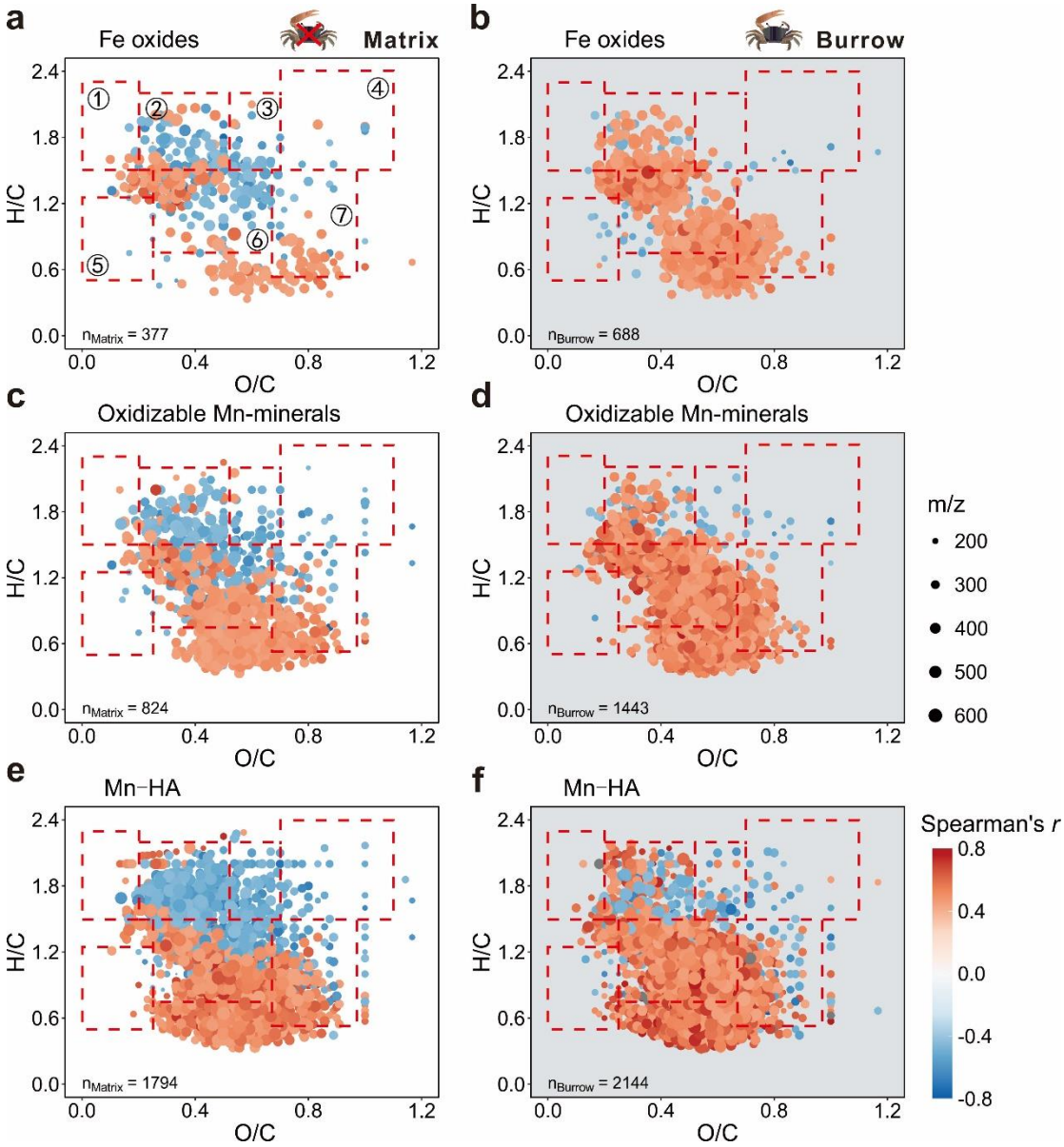

Supplementary Figure 4. | Significant Spearman correlation coefficients ($p < 0.05$) of individual molecules with Fe oxides, oxidizable Mn minerals, and Mn-HA in (a, c, e) the sediment matrix and (b, d, f) crab burrows. The color scale indicates Spearman correlations between the intensity of individual molecules and Fe oxides, oxidizable Mn minerals, and Mn-HA (red: positive; blue: negative). Boxes overlain on the plots indicate major biomolecular compound classes, including: ① lipid-like, ② protein-like, ③ amino sugar-like, ④ carbohydrate-like, ⑤ condensed aromatic-like, ⑥ lignin-like, and ⑦ tannin-like.

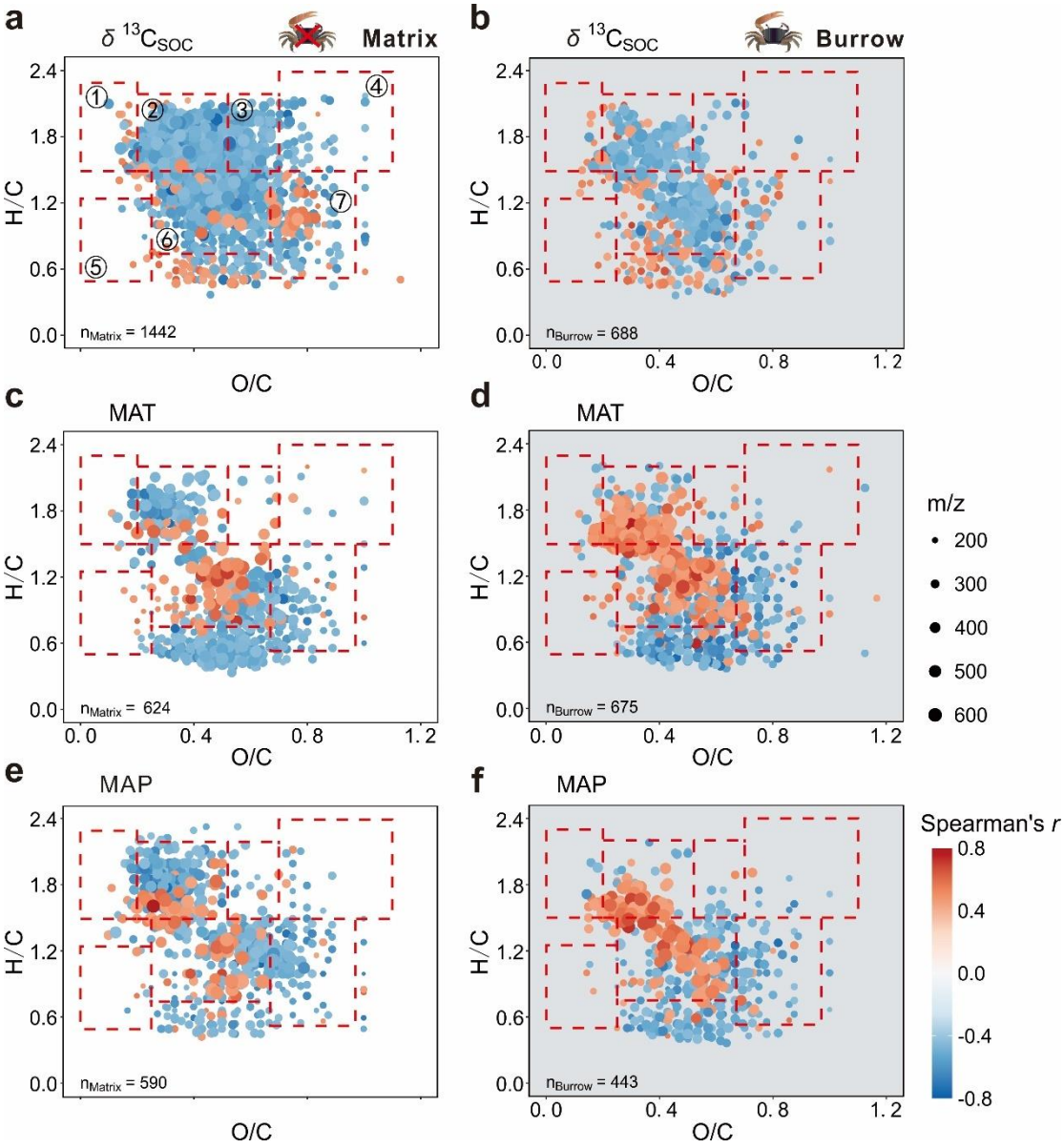

Supplementary Figure 5. | Significant Spearman correlation coefficients ($p < 0.05$) of individual molecules with δ $^{13}C_{SOC}$, manual mean annual temperature (MAT) and mean annual precipitation (MAP) in (a, c, e) sediment matrix and (b, d, f) crab burrows. The left column represents soil matrix samples, and the right column represents burrow samples. The color scale indicates Spearman correlations between the intensity of individual molecules and δ $^{13}C_{SOC}$, MAT, and MAP (red, positive; blue, negative). Boxes overlain on the plots indicate major biomolecular compound classes, including: ① lipid-like, ② protein-like, ③ amino sugar-like, ④ carbohydrate-like, ⑤ condensed aromatic-like, ⑥ lignin-like, and ⑦ tannin-like.

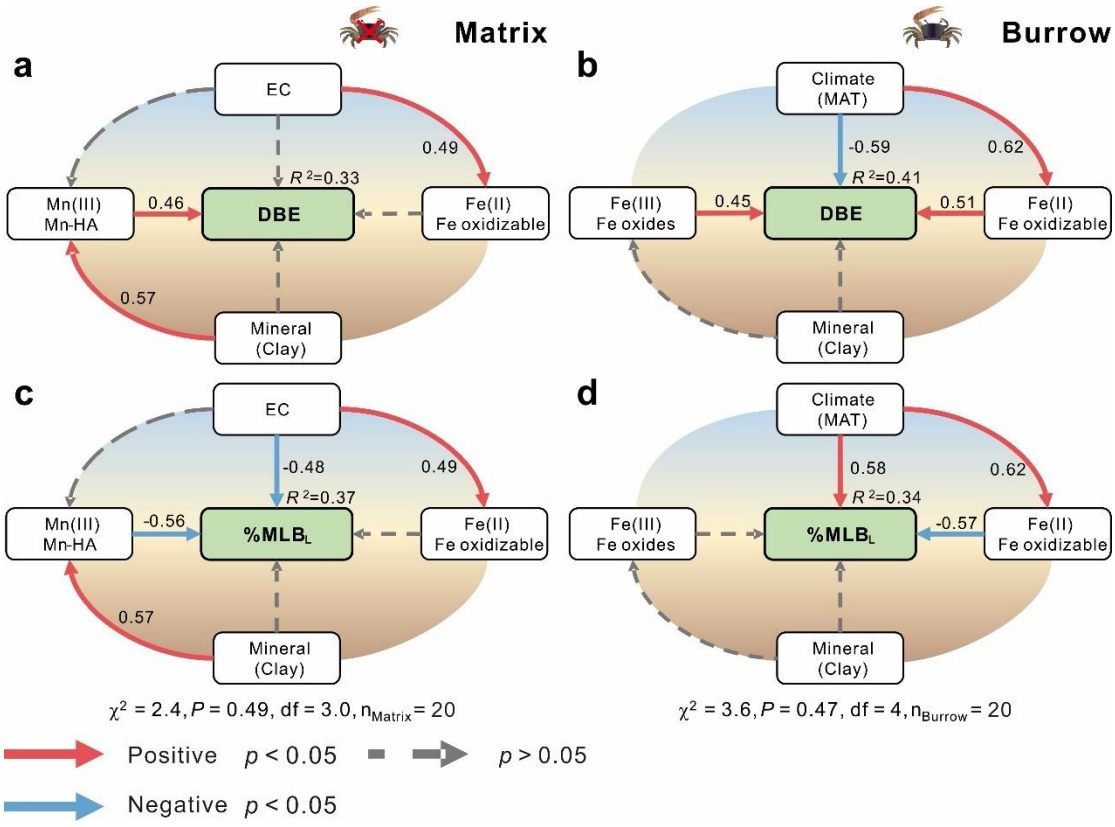

Supplementary Figure 6. | Cascading relationships of DOM marks with environmental factors. Best-supported structural equation models showed major pathways of the influences of environmental factors on (a, b) double-bond equivalent (DBE) (n = 20) and (c, d) molecular lability boundary (%MLB_L) (n = 20). Single-headed arrows indicate the hypothesized direction of causation. Numbers on the red (i.e., positive relationships) and blue (i.e., negative relationships) arrows indicate significant standardized path coefficients at $p < 0.05$, whereas dotted arrows indicate insignificant pathways. The numbers adjacent to the arrows are standardized path coefficients that reflect the relative effect size of the relationship. The goodness-of-fit statistics for the model are presented below.

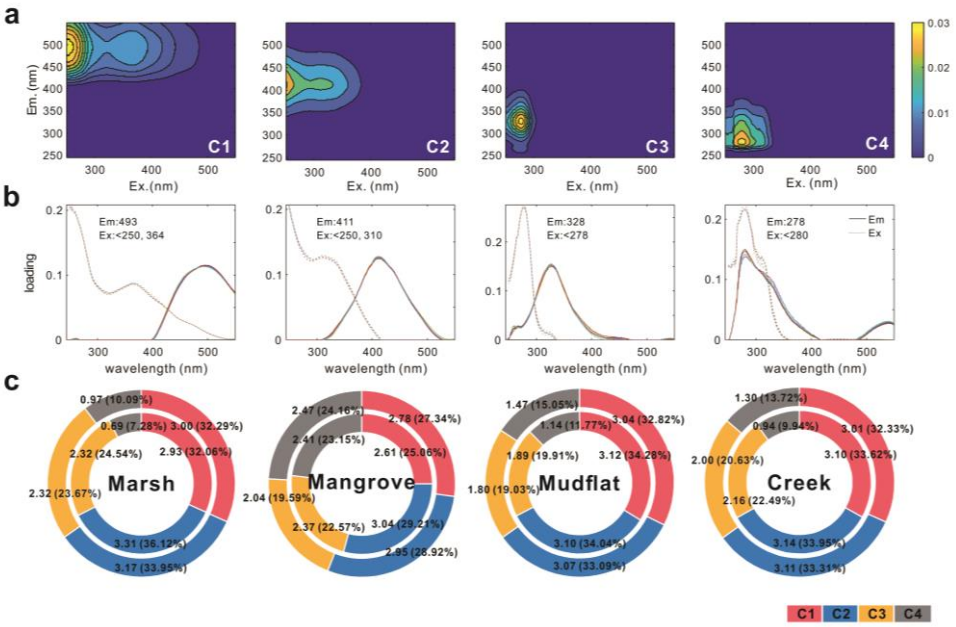

Supplementary Figure 7 | Analysis of dissolved organic matter compositions using Parallel Factor Analysis (PARAFAC) modeling. (a) Contour maps of the four components (C1–C4). Colors represent the relative intensities of the emissions. Dark blue and yellow correspond to the lowest and highest intensities, respectively; (b) line plots for the half validation of excitation and emission loadings; and (c) the average composition of the four components in the PARAFAC models at four crab habitats. The outer and inner circles indicate the matrix and burrow sample, respectively.

Supplementary Table 1 | Longitude, latitude, and habitat type of the sampling site.

NO.	Sites	Habitat type	Longitude	latitude
1	Fangchenggang, Guangxi	Bare mudflat	108°31′09″E	21°35′49″N
1	Fangchenggang, Guangxi	Mangrove	108°31′10″E	21°35′50″N
2	Beihai, Guangxi	Bare mudflat	109°11′37″E	21°25′03″N
2	Beihai, Guangxi	Mangrove	109°11′39″E	21°25′04″N
3	Leizhou, Guangdong	Saltmarsh	110°10′23″E	20°54′04″N
3	Leizhou, Guangdong	Mangrove	110°10′20″E	20°54′04″N
3	Leizhou, Guangdong	Bare mudflat	110°10′24″E	20°54′03″N
3	Leizhou, Guangdong	Creek bank	110°10′34″E	20°53′43″N
4	Yangjiang, Guangdong	Bare mudflat	111°56′10″E	21°42′57″N
4	Yangjiang, Guangdong	Saltmarsh	111°56′11″E	21°42′55″N
4	Yangjiang, Guangdong	Mangrove	111°56′11″E	21°42′54″N
5	Dacheng, Guangdong	Creek bank	117°07′04″E	23°34′14″N
6	Fuzhou, Fujian	Bare mudflat	119°38′13″E	26°01′53″N
6	Fuzhou, Fujian	Saltmarsh	119°38′12″E	26°01′49″N
6	Fuzhou, Fujian	Mangrove	119°38′11″E	26°01′47″N

7	Wenzhou, Zhejiang	Bare mudflat	120°45′11″E	27°43′53″N
7	Wenzhou, Zhejiang	Saltmarsh	120°45′01″E	27°43′55″N
7	Wenzhou, Zhejiang	Creek bank	120°45′02″E	27°43′55″N
8	Taizhou, Zhejiang	Bare mudflat	121°37′17″E	28°20′49″N
8	Taizhou, Zhejiang	Saltmarsh	121°37′14″E	28°20′50″N
8	Taizhou, Zhejiang	Creek bank	121°37′16″E	28°20′53″N
9	Hangzhouwan, Zhejiang	Bare mudflat	121°24′45″E	30°18′59″N
9	Hangzhouwan, Zhejiang	Saltmarsh	121°24′05″E	30°19′14″N
9	Hangzhouwan, Zhejiang	Saltmarsh	121°24′26″E	30°19′06″N
9	Hangzhouwan, Zhejiang	Creek bank	121°24′48″E	30°18′43″N
10	Chongming, Shanghai	Saltmarsh	121°53′35″E	31°27′02″N
10	Chongming, Shanghai	Creek bank	121°53′34″E	31°27′02″N
11	Rudong, Jiangsu	Saltmarsh	121°06′53″E	32°32′29″N
11	Rudong, Jiangsu	Bare mudflat	121°07′15″E	32°32′27″N
12	Dongtai, Jiangsu	Saltmarsh	120°57′27″E	32°40′01″N
12	Dongtai, Jiangsu	Bare mudflat	120°57′41″E	32°39′55″N
13	Xingzhuanghe, Jiangsu	Bare mudflat	119°12′09″E	34°54′08″N
14	Mutaohe, Jiangsu	Bare mudflat	119°12′31″E	35°00′53″N
14	Mutaohe, Jiangsu	Saltmarsh	119°12′35″E	35°00′54″N
15	Weifang, Shandong	Bare mudflat	119°27′13″E	37°06′59″N
15	Weifang, Shandong	Saltmarsh	119°33′03″E	37°05′38″N
15	Weifang, Shandong	Creek bank	119°33′05″E	37°05′47″N
16	Nanhaipu, Shandong	Bare mudflat	118°55′47″E	37°27′42″N
16	Nanhaipu, Shandong	Saltmarsh	118°55′57″E	37°27′32″N
16	Nanhaipu, Shandong	Creek bank	118°56′05″E	37°27′38″N
17	Diaokou, Shandong	Bare mudflat	118°35′40″E	38°05′02″N
17	Diaokou, Shandong	Saltmarsh	118°35′29″E	38°05′12″N
17	Diaokou, Shandong	Creek bank	118°35′04″E	38°05′00″N
18	Cangzhou, Hebei	Bare mudflat	117°45′51″E	38°19′58″N
18	Cangzhou, Hebei	Saltmarsh	117°45′50″E	38°19′45″N
18	Cangzhou, Hebei	Creek bank	117°45′54″E	38°19′50″N
19	Binhaiyuchang, Tianjin	Saltmarsh	117°35′25″E	38°47′38″N
19	Binhaiyuchang, Tianjin	Bare mudflat	117°35′33″E	38°47′47″N
20	Panjin, Liaoning	Bare mudflat	121°40′18″E	40°50′05″N
20	Panjin, Liaoning	Creek bank	121°40′05″E	40°50′11″N
20	Panjin, Liaoning	Saltmarsh	121°40′11″E	40°50′05″N
21	Dandong, Liaoning	Bare mudflat	123°49′53″E	39°49′47″N
21	Dandong, Liaoning	Creek bank	123°49′49″E	39°49′46″N

Supplementary Table 2 | Definitions of the fluorescence and molecular indices.

Parameters	Description
Fluorescence index (FI)	High FI ~ 1.8, derived from extracellular release and leachate from bacteria and algae; low FI ~ 1.2, terrestrial plant and soil organic matter [2].
Slope ratio (S_R)	It usually has a negative correlation with the molecular weight (MW) of DOM [3].
Biological index (BIX)	An indicator of autotrophic productivity. High values correspond to recently produced DOM of autochthonous origin [4].
Humification index (HIX)	Indicator of humic substance content or extent of humification. The HIX is based on the idea that the emission spectra of fluorescing molecules will shift toward longer wavelengths (due to lower H:C ratios) as humification of DOM proceeds. Higher values indicate an increasing degree of humification [5].
Chromophoric dissolved organic matter (CDOM)	A fraction of the DOM pool, sometimes referred to as colored dissolved organic matter [6].
Specific ultraviolet absorbance at 254 nm ($SUVA_{254}$)	Absorbance per unit carbon. Typically, a higher number is associated with greater aromatic content [7].
Degradation index (I_{DEG})	An indicator of degradation. of Higher I_{DEG} values generally correspond to a higher degree of degradation[8].
Island of stability (IOS)	A set of marine dissolved organic compounds with the most stable combination of elements [9].
Double bond equivalent (DBE)	An indicator related with unsaturation of molecule. High values corresponding to high unsaturation [8].
Aromaticity index (AI_{mod})	An indicator of aromaticity. High values indicate high aromaticity of DOM.
Molecular lability boundary (%MLB_L)	An indicator to evaluate the lability of DOM. High values corresponding to high lability [10].
Nominal oxidation state of carbon (NOSC)	An indicator of biogeochemical reactivity and bioavailability, it reflects the thermodynamic stability of organic matter against microbial oxidation [11].
Carboxyl-rich alicyclic molecules (CRAM)	It is usually identified as the dominant oxygen-bearing functional group in marine DOM [12].

Supplementary Note 1. Sediment physicochemical properties

The sediment samples were lyophilized after being transported to the laboratory and stored in plastic boxes at room temperature. The samples were homogenized and passed through a 2 mm sieve before further analyses and DOM extraction experiments. The particle size distribution of the sieved sediments was measured using a laser diffraction particle size analyzer (LS I3 320, Beckman Coulter,

USA).

SOC was determined using the potassium dichromate external heating method. TN_S was determined using the semi-micro Kjeldahl method, and the ratio of SOC to TN_S (C/N ratio) was calculated. The oven-dried soil aggregates were finely ground (< 0.15 mm) before determining the isotopic composition ($\delta^{13}C$). After removing the carbonates with hydrochloric acid (HCl), each fraction was washed with deionized water to remove excess chloride ions. Sediment samples were analyzed for ^{13}C isotopic composition using a GasBench II coupled to a 253 Plus mass spectrometer (Thermo Fischer Scientific) with a measurement error of ± 0.2‰ for $\delta^{13}C_{SOC}$.

The sequential extraction procedure for heavy metals in sediments follows the Geological Survey Technical Standards of the China Geological Survey (DD2005-03) [18, 19]. This scheme was modified from Tessier [20] to avoid the extraction of weakly bound and more reactive fractions from the organic-bound fraction of sediments, which could lead to the overestimation of certain element concentrations. Five morphological extractions were carried out: ion-exchangeable, carbonate-bound, humic acid-bound, iron-manganese oxide-bound, and strong organic-bound fractions. Each extraction step was followed by centrifugation at 3000 rpm for 20 min to separate the extract. The sediments were washed with ultrapure water between different extraction steps to avoid interference from residual reagents. The extracts were then appropriately diluted and analyzed for heavy metal content using inductively coupled plasma mass spectrometry (ICP-MS; PE NexiON 2000). This study used Chinese standard riverine sediment GBW07360 for method validation. The sum of all the extracted fractions was compared with the total element content to ensure data accuracy. The method recovery rates for Fe and Mn were 112.3% and 86.5%, respectively, and the RSDs for each fraction ranged from 4.3% to 23.6%.

Supplementary Note 2. General water quality and DOM optical characterization

Sediment DOM was extracted by shaking 3 g of soil in 60 mL of Milli-Q water at 200 rpm and 20 °C for 24 h. The resulting supernatant was filtered through a polyethersulfone membrane with a pore size of 0.22 μm (Millipore Express® Plus) to obtain the final DOM samples, which were stored at -20 °C prior to further analyses. General water quality was analyzed; specifically, pH was analyzed using a benchtop meter HQ440d and an Intellical™ PHC201 pH probe. The TC, DOC, and TN_W concentrations were measured using a total organic carbon analyzer (TOC-L CSH/CSN analyzer, Shimadzu, Japan). Potassium hydrogen phthalate was used as the standard for calibration, with a linear regression coefficient $R^2 > 0.999$. Approximately 15 mL of the sample was acidified to pH 2.0 by adding at least 30 μL of 6 M hydrochloric acid before DOC analysis. Then, DIC was calculated by subtracting the DOC from TC.

Ultraviolet-visible absorbance spectra were measured using a spectrophotometer (Horiba, Japan). The specific ultraviolet absorbance at 254 nm ($SUVA_{254}$, $L \cdot mg\text{-}C^{-1} \cdot m^{-1}$) was calculated by dividing the UV absorbance at 254 nm (A_{254}) by the DOC concentration, indicating the aromaticity of DOM[7]. The absorption coefficient at 350 nm (a350) was selected as a proxy for chromophoric dissolved organic matter (CDOM) concentration[6]. The ratio of the spectral slope (S_R) measured in the range 275–295 nm to the slope measured in the range 350–400 nm reflects the rate of absorbance change with wavelength, which is usually negatively correlated with the average molecular weight of DOM (R. G. M. Spencer et al., 2012). The groundwater samples were diluted using Milli-Q ultrapure water to an A_{254} less than 0.1, and then fluorescence excitation-emission matrices (EEMs) were measured using an Aqualog spectrofluorometer (Horiba, Japan) with excitation (Ex) and emission (Em) wavelengths ranging from 245 to 826 nm (1 nm intervals) and 240–550 nm (2 nm intervals), respectively. The integration time was set to 3 s. Milli-Q ultrapure water was used as a blank sample to correct Rayleigh scattering and Raman scattering[21]. The biological index (BIX) represents the contribution of newly produced DOM and was calculated as the ratio of the fluorescence signal at an Em of 380 nm to the maximum signal observed in the range of 420–435 nm obtained at an Ex of 310 nm[4]. HIX, a proxy of the humic substance content or extent of humification, was calculated as the peak area at Em 435–480 nm divided by the peak area at Em300–345 nm and that at Em435–480 nm obtained at Ex 254 nm[5]. FI, a parameter for tracking DOM sources from aquatic (high FI of ~1.8, derived from microbial release and leachate) or terrestrial (low FI of ~1.2, terrestrial plant and soil organic matter) environments, was calculated as the ratio of Em at 470 nm to Em520 nm obtained at Ex 370 nm [22]. The fluorescent DOM components for the EEM data were determined by modelling of the parallel factor analysis (PARAFAC) using MATLAB (Vision, 2022a; MathWorks, USA) and validation of split-half analysis [23]. The components were compared to published models using the OpenFluor database (http://www.openfluor.org), with the Tucker congruence coefficient as a similarity criteria [24]. A four-component model explaining 99.5% of the fluorescence variability was selected. The maximum fluorescence intensity for each component was represented by Fmax (in R.U.).

Four fluorescent components of DOM in groundwater were identified based on EEM-PARAFAC analysis, hereafter referred to as components one through four (C1-C4; Figure S2). The C1 (Ex/Em maxima: 250 (364)/493 nm) was identified as a UVC humic-like fluorophore mainly associated with fulvic-like matter, which common to a wide range of freshwater environments [7, 24, 25]. C2 (Ex/Em maxima: 250 (310)/411 nm) was identified as a UVA humic-like fluorophore, which is attributed to peak M. Peak M is related to marine humic substances possibly of bacterial

origin [26-28]. The C3 (Ex/Em maxima: 278/328 nm) and C4 (Ex/Em maxima: 280/278 nm) were close to the traditionally defined tryptophan-like peak T and tyrosine-like peak B, respectively, which have been attributed to autochthonous sources [23, 29-31]. Tryptophan-like may indicate intact proteins or less degraded peptide material, whereas tyrosine-like may indicate more degraded peptide material [32].

Supplementary Note 3. FT-ICR MS measurement

SPE-DOM extracts were mixed with ultrapure water to yield a 1:1 water: methanol ratio (v/v) and DOC concentration of 5 mg C L^{-1}. Samples were directly infused into the ESI unit at a flow rate of 2 μL min-1, with the capillary voltage set to 4.5 kV in negative mode. Ions were accumulated for 0.2 s in the quadrupole unit prior to transfer into the ICR cell, recording 1000 scans in broadband mode using 8 mega word data sets and a scan range of 94 to 2000 Da. Mass spectra were internally calibrated with a reference mass list covering the full detected mass range (mass accuracy < 0.1 ppm) [33]. Molecular formulae above the method detection limit (MDL) were assigned using the ICBM-OCEAN. The MDL was 2.5, the sample junction was in fast join mode (0.5 ppm sample tolerance), and a recalibration tolerance of 0.5 ppm. The Minimum signal to MDL ratio as the backbone for recalibration was 5 using the mean recalibration mode. Molecular formulae were assigned with $^{12}C_{1-50}{}^{1}H_{1-200}{}^{16}O_{1-50}{}^{14}N_{0-4}{}^{32}S_{0-2}P_{0-1}$ with a tolerance of 0.5 ppm in the mass range from 100 to 1000 Da while excluding isotope ratio mismatches above signal to MDL ratios of isotope formulae >6. Isotope tolerance was set to 1000 ‰, and the homologous series network approach was applied (CH_2, CO_2, H_2, H_2O, and O). Molecular formulae containing nitrogen (N), sulphur (S), phosphorus (P), and singlet molecular formulae were excluded. All elemental formulae should meet basic chemical criteria: (1) the number of H atoms should be at least 1/3 of that of C atoms, and no more than 2C + N + 2; (2) the total number of N and H atoms should be even; (3) the H/C value < 3 and the O/C value < 1.5 [34, 35].

Supplementary Note 4. Bioturbation on bulk and optical chemodiversity of dissolved organic matter (DOM) among mangroves, saltmarshes, bare mudflat and creek bank

The effects of fiddler crab bioturbation on the bulk and optical chemodiversity of DOM varied slightly among mangroves, salt marshes, bare mudflats, and creek banks. In mangroves, tryptophan-like compounds (C3) and DIC were 25.3% and 45.0% higher, respectively, in crab burrows than in the sediment matrix (Figure 2c; Supplementary Figure 7). This suggests that bioturbation increases tryptophan-like compounds in mangrove sediments, which can then be rapidly mineralized to dissolve in organic carbon (DIC) [13]. In salt marshes, total nitrogen in sediment (TN_S), sediment

organic carbon (SOC), and dissolved organic carbon (DOC) were significantly higher in burrows than in the matrix ($p < 0.05$), indicating that bioturbation and nitrate (NO^{3-}) enrichment promote the decomposition of more complex carbon forms into simpler ones, making organic matter more accessible to other microbial groups[14]. In bare mudflats and creek banks, unexpectedly lower levels of DOC were observed in crab burrows than in the sediment matrix, whereas other indicators varied by habitat (Figure 2c). In bare mudflats, water-extractable characteristics, such as electrical conductivity (EC), total carbon (TC), and total dissolved nitrogen of water extracts (TN_W), were slightly lower in burrows than in the matrix, while the humification index (HIX) and fluorescence index (FI) were higher in burrows (Figure 2c). These results reflect the rapid microbial mineralization of bioavailable compounds due to crab burrowing activities [15]. The specific ultraviolet absorbance at 254 nm ($SUVA_{254}$) exhibited flushing behavior with hydraulic exchange, and the DOM sources shifted from soluble intracellular materials to decayed plant byproducts [16]. In creek bank, stronger hydraulic exchange and burrow flushing [17] resulted in two times larger aromatic humus ($SUVA_{254}$) in crab burrows than in the matrix (Figure 2)

Supplemenary references

1. Tank SE, Lesack LF, Gareis JA *et al.* Multiple tracers demonstrate distinct sources of dissolved organic matter to lakes of the Mackenzie Delta, western Canadian Arctic. *Limnol Oceanogr*. 2011; **56**(4): 1297-1309. doi: https://doi.org/10.4319/lo.2011.56.4.1297
2. McKnight DM, Boyer EW, Westerhoff PK *et al.* Spectrofluorometric characterization of dissolved organic matter for indication of precursor organic material and aromaticity. *Limnol Oceanogr*. 2001; **46**(1): 38-48. doi: https://doi.org/10.4319/lo.2001.46.1.0038
3. Helms JR, Stubbins A, Ritchie JD *et al.* Absorption spectral slopes and slope ratios as indicators of molecular weight, source, and photobleaching of chromophoric dissolved organic matter. *Limnol Oceanogr*. 2008; **53**(3): 955-969. doi: https://doi.org/10.2307/40058211
4. Wilson HF, Xenopoulos MA. Effects of agricultural land use on the composition of fluvial dissolved organic matter. *Nat Geosci*. 2009; **2**(1): 37-41. doi: https://doi.org/10.1038/ngeo391
5. Ohno T. Fluorescence inner-filtering correction for determining the humification index of dissolved organic matter. *Environ Sci Technol*. 2002; **36**(4): 742-746. doi: https://doi.org/10.1021/es0155276
6. Spencer RG, Butler KD, Aiken GR. Dissolved organic carbon and chromophoric dissolved organic matter properties of rivers in the USA. *J Geophys Res Biogeosci*. 2012; **117**(G3). doi: https://doi.org/10.1029/2011JG001928
7. Weishaar JL, Aiken GR, Bergamaschi BA *et al.* Evaluation of specific ultraviolet absorbance as an indicator of the chemical composition and reactivity of dissolved organic carbon. *Environ Sci Technol*. 2003; **37**(20): 4702-4708. doi: 10.1021/es030360x
8. Flerus R, Lechtenfeld O, Koch BP *et al.* A molecular perspective on the ageing of marine dissolved organic matter. *Biogeosciences*. 2012; **9**(6): 1935-1955. doi: https://doi.org/10.5194/bg-9-1935-2012
9. Hertkorn N, Ruecker C, Meringer M *et al.* High-precision frequency measurements: indispensable tools at the core of the molecular-level analysis of complex systems. *Anal Bioanal Chem*. 2007; **389**:

1311-1327. doi: https://doi.org/10.1007/s00216-007-1577-4
10. D'Andrilli J, Cooper WT, Foreman CM *et al.* An ultrahigh-resolution mass spectrometry index to estimate natural organic matter lability. *Rapid Commun Mass Spectrom*. 2015; **29**(24): 2385-2401. doi: https://doi.org/10.1002/rcm.7400
11. Kellerman AM, Kothawala DN, Dittmar T *et al.* Persistence of dissolved organic matter in lakes related to its molecular characteristics. *Nat Geosci*. 2015; **8**(6): 454-457. doi: https://doi.org/10.1038/ngeo2440
12. Hertkorn N, Benner R, Frommberger M *et al.* Characterization of a major refractory component of marine dissolved organic matter. *Geochim Cosmochim Acta*. 2006; **70**(12): 2990-3010. doi: https://doi.org/10.1016/j.gca.2006.03.021
13. Wei J, Zhang F, He T *et al.* Selective associations of organic matter components with ferrihydrite: Implications for Fe-organic matter preservation in tidal flat wetlands. *Geoderma*. 2023; **437**: 116574. doi: https://doi.org/10.1016/j.geoderma.2023.116574
14. Bulseco AN, Giblin AE, Tucker J *et al.* Nitrate addition stimulates microbial decomposition of organic matter in salt marsh sediments. *Glob Change Biol*. 2019; **25**(10): 3224-3241. doi: https://doi.org/10.1111/gcb.14726
15. Gunina A, Kuzyakov Y. From energy to (soil organic) matter. *Glob Chang Biol*. 2022; **28**(7): 2169-2182. doi: https://doi.org/10.1111/gcb.16071
16. Roebuck Jr JA, Prestegaard Jr K, Gaviria C *et al.* Hydrobiogeochemical controls on the delivery of dissolved organic matter to boreal headwater streams. *Water Resour Res*. 2023; **59**(10): e2022WR033358. doi: https://doi.org/10.1029/2022WR033358
17. Xiao K, Wilson AM, Li H *et al.* Large CO_2 release and tidal flushing in salt marsh crab burrows reduce the potential for blue carbon sequestration. *Limnol Oceanogr*. 2021; **66**(1): 14-29. doi: https://doi.org/10.1002/lno.11582
18. Liu W, Ma L, Liu H *et al.* Reasearch on Speciation Analysis of Chemical Elements in Soil Samples for Ecosystem Geochemistry Study (in Chinses). *ROCK AND MINERAL ANALYSIS*. 2005; **03**: 181-188. doi: https://doi.org/CNKI:SUN:YKCS.0.2005-03-004
19. Zha L, Ma L, Liu W *et al.* Morphological Analysis of Elements in Soils Using Mechanical Shaking Extraction and Ultrasonic Vibration Extraction (in Chinses). *ROCK AND MINERAL ANALYSIS*. 2011; **30**(04): 393-399. doi: 10.3969/j.issn.0254-5357.2011.04.003
20. Tessier* A, Campbell PGC, Bisson M. Sequential Extraction Procedure for the Speciation of Particulate Trace Metals. *Analytical Chemistry*. 1979; **51**(7): 845.
21. Murphy KR, Butler KD, Spencer RG *et al.* Measurement of dissolved organic matter fluorescence in aquatic environments: an interlaboratory comparison. *Environ Sci Technol*. 2010; **44**(24): 9405-9412. doi: https://doi.org/10.1021/es102362t
22. Cory RM, McKnight DM. Fluorescence spectroscopy reveals ubiquitous presence of oxidized and reduced quinones in dissolved organic matter. *Environ Sci Technol*. 2005; **39**(21): 8142-8149. doi: https://doi.org/10.1021/es0506962
23. Murphy KR, Stedmon CA, Graeber D *et al.* Fluorescence spectroscopy and multi-way techniques. PARAFAC. *Anal Methods*. 2013; **5**(23): 6557-6566. doi: 10.1039/c3ay41160e
24. Murphy KR, Stedmon CA, Wenig P *et al.* OpenFluor–an online spectral library of auto-fluorescence by organic compounds in the environment. *Anal Methods*. 2014; **6**(3): 658-661. doi: https://doi.org/10.1039/c3ay41935e

25. Walker SA, Amon RM, Stedmon CA. Variations in high-latitude riverine fluorescent dissolved organic matter: A comparison of large Arctic rivers. *J Geophys Res Biogeosci*. 2013; **118**(4): 1689-1702. doi: https://doi.org/10.1002/2013JG002320

26. Cawley KM, Ding Y, Fourqurean J *et al.* Characterising the sources and fate of dissolved organic matter in Shark Bay, Australia: a preliminary study using optical properties and stable carbon isotopes. *Mar Freshw Res*. 2012; **63**(11): 1098-1107. doi: https://doi.org/10.1071/mf12028

27. Catalá TS, Reche I, Fuentes-Lema A *et al.* Fluorescent dissolved organic matter in the dark global Ocean. 2013. doi: https://doi.org/10.1038/ncomms6986

28. Graeber D, Gelbrecht J, Pusch MT *et al.* Agriculture has changed the amount and composition of dissolved organic matter in Central European headwater streams. *Sci Total Environ*. 2012; **438**: 435-446. doi: https://doi.org/10.1016/j.scitotenv.2012.08.087

29. Kothawala DN, Stedmon CA, Müller RA *et al.* Controls of dissolved organic matter quality: Evidence from a large-scale boreal lake survey. *Glob Chang Biol*. 2014; **20**(4): 1101-1114. doi: https://doi.org/10.1111/gcb.12488

30. Shutova Y, Baker A, Bridgeman J *et al.* Spectroscopic characterisation of dissolved organic matter changes in drinking water treatment: From PARAFAC analysis to online monitoring wavelengths. *Water Res*. 2014; **54**: 159-169. doi: https://doi.org/10.1016/j.watres.2014.01.053

31. Hambly A, Arvin E, Pedersen L-F *et al.* Characterising organic matter in recirculating aquaculture systems with fluorescence EEM spectroscopy. *Water Res*. 2015; **83**: 112-120. doi: https://doi.org/10.1016/j.watres.2015.06.037

32. Murphy KR, Ruiz GM, Dunsmuir WT *et al.* Optimized parameters for fluorescence-based verification of ballast water exchange by ships. *Environ Sci Technol*. 2006; **40**(7): 2357-2362. doi: https://doi.org/10.1021/es0519381

33. Seidel M, Vemulapalli SPB, Mathieu D *et al.* Marine dissolved organic matter shares thousands of molecular formulae yet differs structurally across major water masses. *Environ Sci Technol*. 2022; **56**(6): 3758-3769. doi: https://doi.org/0.1021/acs.est.1c04566

34. He C, Zhang Y, Li Y *et al.* In-house standard method for molecular characterization of dissolved organic matter by FT-ICR mass spectrometry. *ACS omega*. 2020; **5**(20): 11730-11736. doi: https://doi.org/10.1021/acsomega.0c01055

35. Kujawinski EB, Behn MD. Automated analysis of electrospray ionization Fourier transform ion cyclotron resonance mass spectra of natural organic matter. *Anal Chem*. 2006; **78**(13): 4363-4373. doi: https://doi.org/10.1021/ac0600306